analytical chemistry

Article

Cite This: Anal. Chem. XXXX, XXX, XXX−XXX

pubs.acs.org/ac

Development of a High-Resolution Laser Absorption Spectroscopy Method with Application to the Determination of Absolute Concentration of Gaseous Elemental Mercury in Air

Abneesh Srivastava* and Joseph T. Hodges

Chemical Sciences Division, National Institute of Standards and Technology, 100 Bureau Drive, Gaithersburg, Maryland 20899-8393, United States

Supporting Information

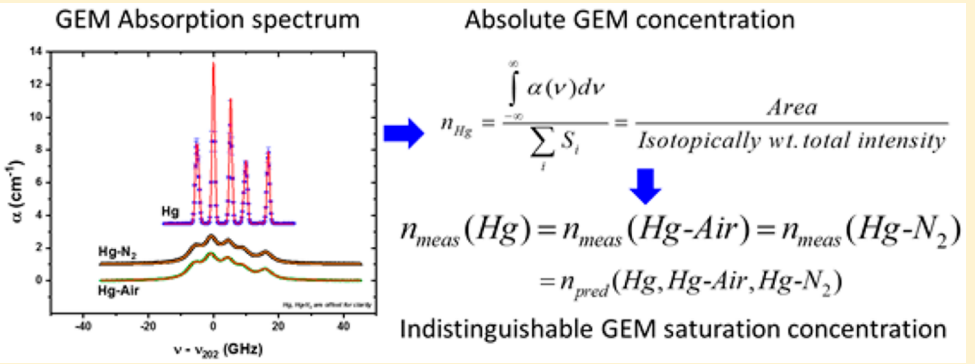

ABSTRACT: Isotope dilution-cold-vapor-inductively coupled plasma mass spectrometry (ID-CV-ICPMS) has become the primary standard for measurement of gaseous elemental mercury (GEM) mass concentration. However, quantitative mass spectrometry is challenging for several reasons including (1) the need for isotopic spiking with a standard reference material, (2) the requirement for bias-free passive sampling protocols, (3) the need for stable mass spectrometry interface design, and (4) the time and cost involved for gas sampling, sample processing, and instrument calibration. Here, we introduce a high-resolution laser absorption spectroscopy method that eliminates the need for sample-specific calibration standards or detailed analysis of sample treatment losses. This technique involves a tunable, single-frequency laser absorption spectrometer that measures isotopically resolved spectra of elemental mercury (Hg) spectra of 6 $^1S_0 \leftarrow 6\ ^3P_1$ intercombination transition near $\lambda = 253.7$ nm. Measured spectra are accurately modeled from first-principles using the Beer−Lambert law and Voigt line profiles combined with literature values for line positions, line shape parameters, and the spontaneous emission Einstein coefficient to obtain GEM mass concentration values. We present application of this method for the measurement of the equilibrium concentration of mercury vapor near room temperature. Three closed systems are considered: two-phase mixtures of liquid Hg and its vapor and binary two-phase mixtures of Hg−air and Hg−N_2 near atmospheric pressure. Within the experimental relative standard uncertainty, 0.9−1.5% congruent values of the equilibrium Hg vapor concentration are obtained for the Hg-only, Hg−air, Hg−N_2 systems, in confirmation with thermodynamic predictions. We also discuss detection limits and the potential of the present technique to serve as an absolute primary standard for measurements of gas-phase mercury concentration and isotopic composition.

There are three forms[1,2] of atmospheric mercury: gaseous elemental mercury, Hg^0 (GEM), divalent gaseous mercury (Hg(II)), and particle-bound mercury (Hg-p). The majority (95%) of the gaseous mercury is in the form of Hg^0, which makes the emission, transport, and toxicology of GEM an important species in atmospheric science studies.[3] GEM emissions arise from a combination of anthropogenic and natural geogenic primary sources and secondary re-emission sources originating from surface reservoirs.[3] GEM has an atmospheric lifetime of 0.5−1 year,[4] allowing it to be transportable and prone to bioaccumulation.[1,5] Mercury is classified as a neurotoxin,[6,7] and it is regulated by the United States Environmental Protection Agency (U.S. EPA) and other global government agencies as a potent hazardous pollutant.[8,9] The environmental and occupational health standards for inhalation exposure to mercury vapor range over 0.3−100 $\mu g\ m^{-3}$, classified based on time, threshold, and trigger for investigation.[10]

In order to quantify mercury emissions in the field, continuous emission monitoring systems comprising a calibration GEM generator unit and cold-vapor atomic absorption or fluorescence spectroscopy analyzers (CVAAS, CVAFS) unit are commonly employed.[11] GEM generators are open systems that involve a metered carrier gas (typically air or

Received: February 14, 2018
Accepted: April 30, 2018
Published: April 30, 2018

DOI: 10.1021/acs.analchem.8b00757
Anal. Chem. XXXX, XXX, XXX−XXX

N_2) in equilibrium with a reservoir of liquid Hg at a controlled temperature. In principle, this approach, provides a GEM mass concentration that depends only on the partial pressure of the liquid mercury and the total flow rate of the carrier gas. In practice, temperature and flow rate are used to precisely control the amount of GEM in the carrier gas, and linkage to the Système International d'unités (SI) is realized through a chain of calibrations to an SI-traceable primary standard for elemental mercury mass concentration.

In the USA, primary standard generators for mercury mass concentration are used to certify commercial standard generators to which field-deployed GEM systems are typically certified. The primary standard generators used for these certifications, which are located at the National Institute of Standards and Technology (NIST) in Gaithersburg, MD span the mass concentration range 0.25−300 $\mu g\ m^{-3}$ for GEM and are in turn characterized by SI-traceable measurements of mercury mass and carrier gas volume. Specifically, the mass of mercury emitted by the NIST primary standard generators is measured using an isotope-dilution-inductively coupled mass spectrometry (ID-ICPMS) method that is referenced to an SI standard for mercury amount-of-substance (NIST SRM 3133).[12] Using this scheme, certifications of NIST primary standard generators have relative standard uncertainties between 1% and 2% for GEM mass concentration.

Although mass spectrometric measurements of collected mercury result in acceptable accuracy for characterizing the output of the NIST standard generators, the overall approach is time-consuming, labor intensive, and costly. Therefore, at the expense of introducing additional uncertainty because of unaccounted-for system drift, routine certifications of the NIST standard generators cannot be implemented. Consequently, we seek an alternative approach that is rapid, accurate, and which has the potential for mercury concentration measurement over a wider dynamic range than is currently available. The present strategy involves demonstrating the feasibility of isotope-resolved, ultraviolet (UV) laser absorption spectroscopy of elemental mercury: an SI-traceable, calibration-free method that will be sensitive, rapid, and accurate. Direct absorption of ground state atoms, as adopted in our approach, provides an advantage over excited state-relaxation-based fluorescence detection, which is sensitive to quenching by foreign gas. As discussed below, we project that this technique will measure mercury mass concentrations greater than approximately 0.1 $\mu g\ m^{-3}$ using single-pass absorption cells nominally 1 m in length. Furthermore, combining the high-resolution approach discussed here with path length-enhanced methods such as cavity ring-down spectroscopy (CRDS) of GEM[13−16] will extend the accessible measurement range to ng cm^{-3} concentration levels, which are representative of ambient-level abundances and well outside the capabilities of current standards maintained at NIST.

In addition to developing a new method for measuring the concentration of GEM, this study addresses present discrepancies in the reported temperature dependence of mercury vapor pressure discussed below. To this end, we measure mercury vapor concentration in contact with liquid mercury in the absence as well as in the presence of air or nitrogen. We note that for a variety of reasons, use of an open system containing flowing air saturated with mercury could be prone to transport losses. Possible loss mechanisms include those caused by sampling, incomplete saturation, thermal instability, or chemical reaction, among others. In the following study, we have therefore used closed systems in the form of a static sealed quartz cell loaded with either pure liquid mercury only or liquid mercury in the presence of atmospheric pressure air or nitrogen. This arrangement ensures gaseous elemental mercury stays in continuous equilibrium over a pool of liquid mercury and is enclosed in an optically transparent and chemically inert material. Inclusion of liquid mercury in equilibrium with nitrogen gas near atmospheric pressure gives us a measurement "sample triad". This strategy allows us to screen for the confounding effects of Hg−O_2 photosensitization[17−19] and possible laser fluence population-saturation threshold requirements needed for accurate measurement of the Hg−air system vapor concentration. The resulting detection parameters help minimize, within our experimental uncertainty, the occurrence of these effects by using low ultraviolet laser intensity and is described in the Supporting Information. Our experiments use ultrazero grade commercial source air (synthetic high purity oxygen, nitrogen mixture) for the air buffer gas and are not subject to photosensitization reactions that could occur in the presence of common flue-gas emission components.[18] Because of the high spectral resolution of the measurements, we can account for changes in the spectra caused by collisional effects. This capability enables us to precisely measure relative Hg vapor concentrations in the presence or absence of surrounding air. Furthermore, we can compare our measured absolute mercury vapor concentration values to those predicted by thermodynamic and empirical correlations. This comparison allows us to establish which of these formulas provides the most accurate representation of Hg vapor pressure for Hg−air standard generators.

The remainder of this article is organized as follows. First, we describe the experimental system and the line-by-line spectroscopic model used for data reduction. We present measured and fitted spectra for the Hg-only, Hg−air, andHg−N_2 systems and discuss sources of bias. We discuss spectrometer performance metrics including detection limits, measurement uncertainties, and potential application to absolute mercury isotope ratio measurements. Finally, we report room-temperature measurements of mercury concentration at room temperature for the Hg-only, Hg−air, and Hg−N_2 systems and compare results with literature values and predictions.

EXPERIMENTAL SECTION

We used a commercial, continuous-wave (CW) light source, consisting of a tunable, narrow line width (sub-MHz) laser system to probe the 6 $^1S_0 \leftarrow 6\ ^3P_1$ absorption transitions of elemental mercury near the UV wavelength λ = 253.73 nm. The light source is a tapered-amplifier, fourth harmonic generator (TA-FHG), which comprises an external cavity diode seed laser emitting at λ = 1.015 μm, followed by a semiconductor amplifier and two cascaded second-harmonic generation stages for nonlinear frequency quadrupling to the UV region. The resulting single-frequency output can be continuously scanned over more than 40 GHz and has a short-term line width <500 kHz. The system produces UV laser output power of more than 20 mW with a specified residual intensity noise less than 0.3% of the mean value.

At each spectrum step, the frequency-doubled beam near λ = 507.5 nm is measured with a wavelength meter (1 MHz frequency resolution) and the transmission of the UV laser beam through the sample cell is recorded. The laser and wavelength meter are used in a closed-loop configuration to

DOI: 10.1021/acs.analchem.8b00757
Anal. Chem. XXXX, XXX, XXX−XXX

actively stabilize the probe laser frequency to the desired set point values. Spectral scans were collected over 40(80) GHz at UV frequency steps ranging from 200 MHz to 1 GHz (400 MHz to 2 GHz) depending on the sample system and desired resolution. The laser frequencies at each set point had a standard deviation of approximately 2 MHz over the data collection time. The narrow line width and precise frequency tunability enable the acquisition of highly resolved absorption spectra (MHz-level precision) that were analyzed as discussed below.

The experimental configuration is schematically shown in Figure 1. The mercury vapor absorption cells were custom

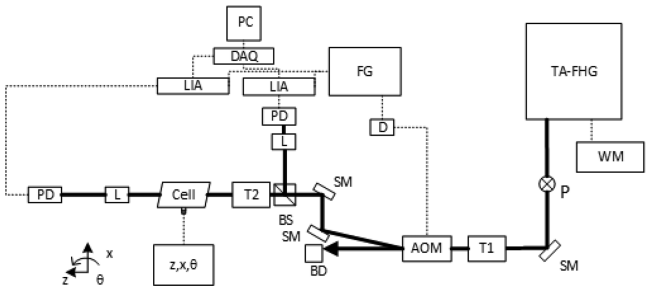

Figure 1. Schematic layout of the optical setup showing the various elements. A tapered amplifier-fourth harmonic generation (TA-FHG) source is coupled to a wavemeter (WM) for frequency scanning. Other elements include steering mirror (SM), telescope (T1, T2), acousto-optic modulator (AOM), rf driver (D), beam dump (BD), beam splitter (BS), lens (L), sample cell, photodiode (PD), lock in amplifier (LIA), function generator (FG), data acquisition (DAQ), and personal computer (PC). Solid lines trace the path of the laser beam, while dashed lines represent electrical and mechanical connections. See text for details.

fabricated to have a quartz cylindrical body with parallel but tilted (2°) faces, thermally sealed with fused silica wedged (2°) windows. This geometry minimized back reflection and etalon effects. The cell path length (nominal value of 10 mm) was measured at several orientations and had an overall relative standard uncertainty of 0.1% about its mean path length (NIST, Dimensional Metrology Group). The cells contained a small volume of liquid mercury localized in a short stem extending below the main cell body. The sensitivity of path length to cell orientation and multiple reflections is provided in the Supporting Information, section S3.

Three separate sealed cells containing mercury in the absence of added gas ($p < 10^{-6}$ Pa), added air (ultrazero grade), and N_2 (99.9999% purity) both at 80 kPa nominal pressure were used for the present studies. These cells contain liquid mercury at a natural isotopic abundance in equilibrium with its vapor in the surrounding gas and are subsequently referred to as Hg-only, Hg−air, and Hg−N_2, respectively. A four-wire industrial platinum resistance thermometer calibrated against an ITS-90 standard platinum resistance thermometer (NIST, Thermodynamic Metrology Group) was used to monitor the cell temperature. All measurements were conducted at room temperature near 22 °C.

The laser beam was intensity modulated with an acousto-optic modulator (AOM) at a modulation frequency of 20 kHz and used in first-order. The intensity-modulated laser beam was expanded and then split into two paths (sample and reference legs), where each path was terminated by a GaP photodiode with a bandwidth of 300 kHz under a load resistance of 1 kΩ and noise-equivalent-power of 13 fW/Hz$^{1/2}$. With this arrangement, the sample path was used to irradiate the sample cell and the reference path was used for signal normalization to compensate for variations in the laser intensity. The sample-path and reference-path photodiode signals were measured using separate phase-sensitive (lock-in) amplifiers, both of which were referenced to the same AOM modulation signal. A multifunction data acquisition device was used to digitize the voltage outputs. Customized software was written to record the signal and control the stepwise frequency tuning of the laser across mercury absorption profile. For saturation characterization studies, the total power and spatial profile of the beam incident on the cell were measured using a calibrated power meter and camera beam profiler, respectively.

SPECTROSCOPIC MODEL

6 $^1S_0$ ← 6 $^3P_1$ Transition Mercury Isotope Absorption Spectra near λ = 253.7 nm. It is well established that the relatively high mercury absorption cross section of the 6 $^1S_0$ ← 6 $^3P_1$ intercombination transition provides an extremely sensitive measurement of mercury concentration.[13−16,20−24] Jongma et al.[14] first demonstrated the application of CRDS to measure GEM concentration by probing this transition. Although, the spectral resolution was limited by the line width of their pulsed laser, $\Delta\nu$ = 7.5 GHz, they were able to demonstrate ultrasensitive detection of GEM in ambient air at a molar fraction of 7 pmol mol^{-1}. Subsequently, Fain et al.[13] developed a prototype CRDS spectrometer using a pulsed laser with a line width of 0.9 GHz which enabled them to resolve the Doppler-broadened spectra of mercury and to achieve a detection limit of 0.04 pmol mol^{-1} for an averaging time of 1 s. This work was extended by Pierce et al.[15] to incorporate a frequency-locked probe laser with the CRDS method for automated field-deployable measurement of GEM.

The emergence of narrow line width, tunable CW diode lasers combined with nonlinear frequency conversion schemes for the generation of UV radiation has enabled measurements of the 6 $^1S_0$ ← 6 $^3P_1$ intercombination transition with improved spectral resolution well below the 1 GHz level. Specifically, Alnis et al.[21] were the first to resolve the Doppler-broadened mercury isotope lines at 253.7 nm. They used sum frequency generation (SFG) of visible diode laser beams to generate 1 nW of UV power at 254 nm with a tuning range of 35 GHz. Carruthers et al.[23] significantly improved the SFG conversion efficiency achieving output powers of 50 nW and demonstrated a tuning range of 70 GHz which allowed them to probe both the Doppler- and air-broadened spectra of mercury with a resolution of approximately 10 MHz. Anderson et al.[22] subsequently developed a ruggedized diode-laser-based sensor package for mercury detection at 253.7 nm. Their system achieved a rapid spectral scan rate (up to 4 kHz) as well as a tuning range of 100 GHz to fully capture the air-broadened absorption spectra of mercury. Based on an inspection of published spectra, Anderson et al. demonstrated the highest spectral resolution and signal-to-noise ratio (SNR) when compared to Alnis et al. and Carruthers et al. More recently Lou et al.[24] used a frequency-doubled multimode diode laser as a simple and rugged laser source. However, for quantitative measurements, the multimode character of the probe laser required a sample-reference cell configuration to extract the concentration of GEM. The potential for long- term (14 h) frequency stabilization and signal averaging was recently

DOI: 10.1021/acs.analchem.8b00757
Anal. Chem. XXXX, XXX, XXX−XXX

exploited by Almog et al.[20] using Doppler-free saturation spectroscopy of this transition.

As discussed below, the absorption spectrum of pure mercury vapor at room temperature and natural isotopic abundance for the $6\ ^1S_0 \leftarrow 6\ ^3P_1$ intercombination transition exhibits six peaks originating from a total of 10 transition lines spanning approximately 22 GHz (Supporting Information, section S1). When the mercury vapor mixes with a bath gas such as air or N_2 the spectrum (as will be shown) the spectrum is dramatically altered due to pressure-broadening-induced blending of individual component transitions.

Beer–Lambert Law and Signal Analysis. We begin by assuming that the composite absorption spectrum can be modeled from first-principles using the Beer–Lambert law, which relates the absorption coefficient, $\alpha(\nu)$, to the product of the absorber number density, n, times its local cross section $\sigma(\nu)$, where ν is the optical frequency.

The dual-path arrangement of Figure 1 yields a pair of electronic signals s_r and s_s, which correspond to the reference and signal channels, respectively. Assuming that the reference photoreceiver responds linearly to the laser irradiation, then $s_r = P_i\varepsilon_r\mathcal{R}_r$, in which P_i is the beam power at the location where the incident beam splits into the two paths, ε_r is the fraction of this power that reaches the reference detector, and $\mathcal{R}_r$ is the transimpedance gain of the reference detector and phase-sensitive amplifier system. Similarly, for the sample channel and in the absence of absorption, then $s_s = P_i\varepsilon_s\mathcal{R}_s$. For an absorbing sample of path length l, the Beer–Lambert law gives the transmittance as $T_s = \exp(-\alpha(\nu)l)$. Dividing the sample signal by the reference signal yields the normalized transmission signal as

$$z(\nu) = \frac{s_s}{s_r} = \frac{P_i\varepsilon_s\mathcal{R}_s \exp(-\alpha(\nu)l)}{P_i\varepsilon_r\mathcal{R}_r} \simeq \beta(1 + \kappa\Delta\nu_1)\exp(-\alpha(\nu)l) \tag{1}$$

in which β and κ are measured system constants and $\Delta\nu$ is the frequency detuning relative to the first point of the scan. Here, β and κ are obtained by the first-order Taylor series expansion of the ratio $(\varepsilon_s\mathcal{R}_s/\varepsilon_r\mathcal{R}_r) = f(\Delta\nu)$ such that $\beta = f(\Delta\nu = 0)$ and $\kappa = (df/d\nu)_{\Delta\nu=0}/f(0)$. The latter quantity accounts for any small difference in the frequency dependence of the collection and measurement efficiencies between the two paths that leads to imperfect normalization. Physical mechanisms contributing to this complication include slight variations in beam steering, reflection efficiencies, and etalons, etc. as the laser frequency is tuned. This term can also capture slowly varying wavelength-dependent losses like Rayleigh scattering and the wings of distant absorption lines by species such as O_2. We also note that spectra acquired with a similar-sized but empty cell also were conducted to rule out the contribution of any absorption features from the cell and air medium.

For optically thin conditions that correspond to the limit $\alpha l \ll 1$, then one can rewrite the exponential term in eq 1 as $\exp(-\alpha l) \approx 1 - \alpha l$. With this assumption, eq 1 can be rearranged to yield

$$\alpha(\nu) = \frac{1}{l}\left(1 - \frac{z(\nu)}{\beta(1 + \kappa\Delta\nu)}\right) \tag{2}$$

in which the absorption coefficient reduces to a linear function of the normalized transmission signal.

The absorption coefficient for a single mercury transition (labeled i) located at frequency $\nu_i = \nu_{0,i} + \Delta\nu_{s,i}$ (here $\nu_{0,i}$ is vacuum line position and $\Delta\nu_{s,i}$ is the pressure shift) can be written as the product of the total mercury number density n_{Hg}, the isotopically weighted line strength S_i, and the line shape function, $\varphi_i(\nu - \nu_i)$ as

$$\alpha_i(\nu - \nu_i) = n_{Hg}S_i\varphi_i(\nu - \nu_i) = n_{Hg}\frac{\chi_i A_{21}c^2}{8\pi{\nu_{0,i}}^2}\left(\varepsilon_i\left(\frac{g_{2,i}}{g_{1,i}} + 1\right) - 1\right)\varphi_i(\nu - \nu_i) \tag{3}$$

in which A_{21} is the Einstein coefficient for spontaneous emission of radiation, c is the speed of light, χ_i is the relative abundance of the isotope, ε_i is the fraction of the isotope population in the ground state, and $g_{2,i}/g_{1,i}$ is the ratio of excited and ground state degeneracies determined from angular momentum quantum numbers.[25] At low fluences and room temperature, $\varepsilon_i \to 1$, so that the absorption coefficient becomes nearly independent of beam intensity (linear absorption regime). In this limit, the line intensity of the transition i can be written as

$$S_i = \frac{\chi_i A_{21}c^2}{8\pi{\nu_{0,i}}^2}\frac{g_{2,i}}{g_{1,i}} \tag{4}$$

and because the line shape functions are integrally normalized to unity (i.e., $\int_{-\infty}^{\infty}\varphi_i(\nu - \nu_i)\,d\nu = 1$), then

$$n_i = \frac{1}{S_i}\int_{-\infty}^{\infty}\alpha_i(\nu - \nu_i)\,d\nu \tag{5}$$

where n_i is the number density of the isotope associated with transition i. Thus, collisional broadening will not alter the total absorption area of a given transition at fixed isotope number density.

A similar result can be obtained for the total intensity obtained by linear superposition of the component absorption coefficients as

$$\alpha(\nu) = \sum_i \alpha_i(\nu) = \frac{n_{Hg}A_{21}c^2}{8\pi}\sum_i \frac{\chi_i}{{\nu_{0,i}}^2}\frac{g_{2,i}}{g_{1,i}}\varphi_i(\nu - \nu_i) \tag{6}$$

where the summation is over these 10 Hg transitions (Supporting Information, section S1). Integration of the composite spectral absorption coefficient over frequency reduces to the product of total mercury number density and isotopically weighted total intensity, $S_{tot} = \sum_i S_i$, so that

$$\int_{-\infty}^{\infty}\alpha(\nu)\,d\nu = \frac{n_{Hg}A_{21}c^2}{8\pi}\sum_i \frac{\chi_i}{{\nu_{0,i}}^2}\frac{g_{2,i}}{g_{1,i}} = n_{Hg}\sum_i S_i = n_{Hg}S_{tot} \tag{7}$$

All line shape functions were modeled using the Voigt profile (VP), which represents a convolution of the Doppler and Lorentzian profiles. The VP accounts for temperature-dependent Doppler broadening as well as collisional mechanisms that broaden and shift the line shape. Input parameters to the VP include the Doppler width $\Delta\nu_D$, the pressure-broadened width $\Delta\nu_c$, and the pressure shift $\Delta\nu_s$ of line center. The Doppler full-width at half-maximum (fwhm) is $\Delta\nu_D = \frac{2\nu_0}{c}\sqrt{\frac{2\ln(2)k_BT}{m}}$ where

DOI: 10.1021/acs.analchem.8b00757
Anal. Chem. XXXX, XXX, XXX–XXX

m is the isotope atomic mass and k_B is the Boltzmann constant. The collisional halfwidth and shift terms are modeled as $\Delta\nu_c = \gamma p$ and pressure shift as $\Delta\nu_s = \delta p$, in which γ and δ are the pressure broadening and pressure shifting coefficients, respectively.

EXPERIMENTAL RESULTS AND SPECTROMETER PERFORMANCE

Measured Spectra and Least-Squares Analysis. We fit our spectral model to the measured absorption spectra using a commercial software package which implements the Levenberg–Marquardt, least-squares-minimization algorithm. The fit returns the quantity $n_{Hg}A_{21}l$, which is in turn converted to mass concentration using the ideal gas law and relative atomic mass of mercury (A_r = 200.59),[26] as well as the measured sample length l. We also used the weighted average of 12 prior determinations of the 6 $^1S_0 \leftarrow 6\ ^3P_1$ transition state lifetime $\tau_{21} = 1/A_{21}$, as a best representation, to specify the spontaneous emission Einstein coefficient. The value A_{21} for all the mercury isotopes are treated to be equal, based on the radiative lifetime studies of Halstead et al.[27] on mercury isotopes. Our analysis of these data, which were compiled in Curtis et al.[28] and references therein, yield $A_{21} = 8.41(28) \times 10^6\ s^{-1}$.

Two methods of data reduction were considered to investigate any potential bias in the results caused by the relatively high optical depths which were observed in the present experiments. The two methods involved fitting the modeled transmission signal $z(\nu)$ (given by eq 2) and alternatively fitting $\ln(z(\nu))$ to the data. These approaches involve nonlinear and linear relations, respectively, between the observations given by $z(\nu)$ or $\ln(z(\nu))$ and $\alpha(\nu)$. To ensure consistency between these analyses, we weighted the $\ln(z(\nu))$ data by the inverse of the relative variance of the measurement, s_s^2/σ_s^2, where s_s, σ_s^2 are the data signal and the variance in the baseline signal, respectively. No weighting was required for fits of $z(\nu)$ to the data. We found that there was no significant difference between the retrieved parameters using the two data fitting methods.

There were four floated parameters for the Hg-only sample runs, including the product $n_{Hg}A_{21}l$, a frequency offset, ν_{off} to account for uncertainty in the absolute frequency indicated by the wavelength meter, and the two baseline terms β and κ. We note that this last quantity typically had a value of 1(3)% over the spectral scan range of 40(80) GHz for Hg (Hg–air) data.

In the fitting procedure for the Hg–air and Hg–N_2 spectra, the total gas pressure value was also floated around the nominal fill pressure value of 80 kPa. This is because the amount of air or N_2 in each sample cell was not precisely known. As a constraint on the collisional broadening of the mercury line shapes, we specified the same pressure broadening and shifting coefficients for all transitions. These quantities were estimated from available data[22,29] on Hg–N_2, Hg–air broadening experiments. The retrieved average (standard deviation) of the pressure values from the fits were 69(0.3) and 73(0.5) kPa for the Hg–N_2 and Hg–air samples, respectively.

Representative spectra and fitted spectral profiles for the Hg-only, Hg–air, and Hg–N_2 samples are shown in Figures 2 and 3, respectively. The results are plotted in terms of absorption coefficient versus frequency detuning expressed as $\Delta\nu = \nu - \nu_{202}$, where ν_{202} is the measured line center of the ^{202}Hg absorption line.

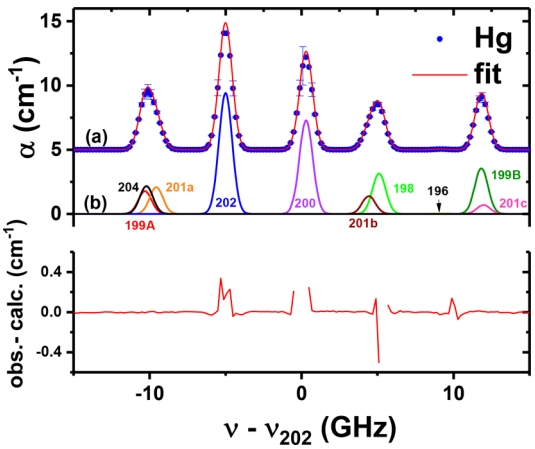

Figure 2. Top panel: (a) measured (symbols) and fitted absorption coefficient for mercury vapor at room temperature with no added gas ($p < 10^{-6}$ Pa) based on weighted fit to $\ln(z)$, where z is the measured transmission given by eq 1. The data and fit have been offset by 5 units for clarity. (b) Simulated spectra for pure mercury vapor at T = 296 K with indicated transitions, including hyperfine structure of the odd isotopes. Bottom panel: fit residuals. Gaps in residual plot represent points where absorption saturation is observed.

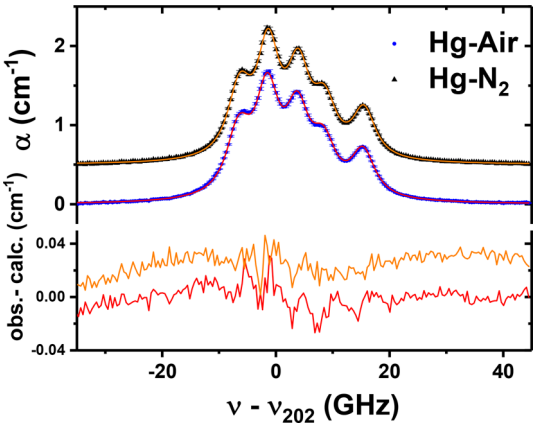

Figure 3. Top panel: (a) measured (symbols) and fitted absorption coefficient for mercury vapor in equilibrium with 73 kPa of air (Hg–air), 69 kPa of N_2 (Hg–N_2) at room temperature. Results are based on weighted fit to $\ln(z)$, where z is the measured transmission given by eq 1. Bottom panel (b): fit residuals. Note, the Hg–N_2 spectrum (residual) is offset by 0.5 (0.025) cm^{-1} along the vertical axis for clarity.

Figure 2 for the Hg-only sample exhibits six resolvable groups, (204, 199A, 201a), (202), (200), (198, 201b), (196), (199B, 201c) of the 10 known allowed transitions. The results are quantitatively consistent with the known transitions of mercury (summarized in Supporting Information, section S1). Because there is a negligible amount of pressure broadening in this case, the individual line shapes are dominated by Doppler broadening with a full-width at half-maximum (fwhm) of nominally 1 GHz. This amount of Doppler broadening is sufficient to cause line blending for the (204, 199A, 201a), (198, 201b), and (199B, 201c) groups, whereas the 202, 200, and 196 amu isotope lines are nearly fully isolated. Given the relatively small number of floated parameters, the quality-of-fit for the composite spectrum is excellent. Over these spectral intervals, the fit residuals exhibit a standard deviation between 0.0015 and 0.005 cm^{-1}.

DOI: 10.1021/acs.analchem.8b00757
Anal. Chem. XXXX, XXX, XXX–XXX

Measured and fitted absorption spectra for the Hg−air and Hg−N_2 samples are shown in Figure 3. Both sets of data exhibit significant pressure broadening and line blending compared to the Hg-only sample, resulting in substantially smaller maximum optical depth. Nevertheless, five peaks are observed, dominated by the 202 and 200 amu isotope transitions. The spectral residuals (observed − fit) were evaluated to obtain a quality-of-fit (QF) parameter, defined as the peak absorption divided by the standard deviation of the fit residuals.[30] This figure-of-merit can be interpreted as the SNR with which a line shape is fitted to experimental data and has values of 197 and 210 for the Hg−air and Hg−N_2 cases, respectively. The regime of saturation and photoreaction bias is covered in the Supporting Information, section S2.

Detection Limit and Spectrometer Dynamic Range. The quantitative nature of the present technique demonstrated above enables us to project how the mercury detection limit and the measurement dynamic range (ratio of maximum to minimum measurable mercury number density) depend upon spectrometer figures-of-merit such as sample length, baseline noise, spectrum sampling density, etc. Here, we define a theoretical detection limit for mercury number density $n_{Hg,min}$ to be the ratio of the minimum measurable spectrum area divided by the isotopically total intensity. To estimate the minimum measurable spectrum area, we invoke a statistical model where we treat the baseline absorption coefficient spectrum, $\Delta\alpha(\nu)$, as Gaussian random noise with a mean value of 0 and standard deviation given by σ_α. With these assumptions, numerical simulations show that for spectra comprising N_p points that are separated by frequency steps $\Delta\nu$ then,

$$n_{Hg,min} = \frac{<\left|\int \Delta\alpha(\nu)\, d\nu\right|>}{S_b} \approx 0.8\frac{(\sigma_\alpha/\sqrt{N_p})\Delta\nu}{S_b} \quad (8)$$

where the integration is over the spectral range $N_p\Delta\nu$, the notation $\langle|\cdots|\rangle$ indicates an ensemble average over the absolute value of the argument, and the approximation symbol indicates strong statistical correlation which yields an approximate factor 0.8 when N_p is large. This result shows that although the ensemble average could be determined by fitting multiple spectra, a similar result can be obtained from a single-spectrum-determination of σ_α.

In Figure 4a, we summarize the dependence of the detection limit for Hg−air or Hg−N_2 samples on the product $\sigma_\alpha l$, assuming a N_p = 50 and $\Delta\nu$ = 0.4 GHz. For the present system with a 1 cm sample length, we estimate a mercury mass concentration detection limit of the order 0.1 μg m^{-3}. This limit can be reduced by several approaches, including increasing the sample length or reducing the baseline noise level through active control of the probe laser intensity and signal averaging.

Simulated spectra for Hg-in-air shown in Figure 4b, also illustrate how the dynamic range of the spectrometer can be extended by operating over a wide range of gas pressure. Provided the gas pressure is well-regulated and accurately measured, this additional degree of freedom will enable spectra to be acquired over a wider concentration range by comparison to measurements made at constant pressure. At fixed molar fraction of mercury, a 10-fold reduction in the pressure reduces the peak absorption by a much smaller factor equal to ≈2.5. Thus, for a given maximum spectrum signal-to-noise ratio (which scales with the quantity α/σ_α), the dynamic range of the measurement will be 2.5 times greater given a 10-fold range in gas pressure. The extra degree-of-freedom afforded by variable pressure will help compensate for reduced peak losses as concentration levels decrease.

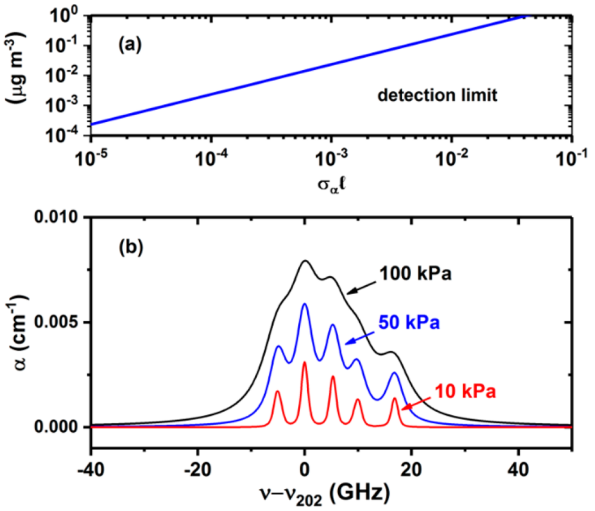

Figure 4. (a) Estimated mercury concentration detection limit vs the product of absorption coefficient baseline standard deviation and sample length. Results are based on eq 8 assuming N_p = 50 and $\Delta\nu$ = 0.4 GHz. (b) Calculated absorption spectra for a Hg−air mixture at T = 296 K for the indicated gas pressures and constant molar fraction, x_{Hg}. Mercury mass concentration at p = 101.325 kPa equal to ρ_{Hg} = 100 μg m^{-3} and x_{Hg} = 12.1 nmol/mol.

Measurement of Absolute Isotopic Composition. Although advances in ICPMS technology in the late 1990s enabled sensitive measurements of parts-per-thousand (per mil, ‰) variations in the relative abundance of mercury isotopes, the determination of absolute isotope ratios for these species remains a significant challenge in analytical chemistry.[31] The existing methods,[31,32] which achieve 0.05‰ and 0.08‰ precision for the $^{202/200}$Hg and $^{202/198}$Hg ratios, respectively, require calibration against a thallium isotopic standard and are subject to bias of up to 5‰ because of mass-bias effects.

As an alternative approach to ICPMS, the precision and isotopic discrimination of the present laser-absorption method may provide a calibration-free approach to measure the absolute isotopic composition of elemental mercury. Typical variations in $^{202/198}$Hg are known to be as large as ±4‰: a variability suggesting that a relative measurement precision no worse than 1‰ in peak area ratio would be required to quantify relevant excursions in isotopic abundance values. Although we found that the fit precision for the ^{200}Hg and ^{202}Hg peak areas, gave a relative uncertainty equal to 4‰, there is substantial room for improvement through increased spectral density, signal averaging, and operation at reduced optical density of ∼0.1 to improve the signal-to-noise ratio of the measured spectra in the region of the line cores. Calculations based on the detection limit given in eq 8 indicate a potential measurement precision at the 0.1‰ level based on a 2 GHz spectral window with 100 spectral points and baseline-noise limited performance at the $\sigma_\alpha = 5 \times 10^{-3}$ cm^{-1} level.

Uncertainty Analysis. The uncertainty calculation for the measurements of the mercury mass concentration was performed per the ISO/JGCM *Guide to the Expression of Uncertainty in Measurement*.[33] Details of the uncertainty calculation are provided in the Supporting Information, section S4. An overall combined relative standard uncertainty, $u_c(n)/n$

DOI: 10.1021/acs.analchem.8b00757
Anal. Chem. XXXX, XXX, XXX−XXX

% of 1.3%, 1.5%, and 0.9% is obtained for Hg-only, Hg−air, Hg−N_2 samples, respectively. The three principal contributors to the uncertainty values are the variability in the measurement data set (type A), sensitivity of Hg number density to the calibration temperature uncertainty (type B), and the uncertainty in the Einstein coefficient, A_{21} (type B). Their values were (1.2, 1.4, 0.6)%, 0.5%, and 0.4%, respectively for (Hg-only, Hg−air, Hg−N_2) samples.

DISCUSSION

Comparison of Thermodynamic and Empirical Correlations for Mercury Partial Pressure. As described above GEM reference generators produce saturated mercury diluted to desired levels in air, therefore requiring knowledge of the vapor pressure−temperature relationship for computation of the output mercury concentration. A commonly used empirical correlation for the temperature dependence of mercury mass concentration in saturated mixtures of mercury and air was given by Dumarey et al.[34] However, this equation yields a value which is 6.4% lower at room temperature (22 °C) compared to that given by the mercury vapor-correlation equation of Huber et al.[35] The latter correlation, given in the previous section, is based on fitting a thermodynamically constrained model over a wide temperature range to numerous mercury vapor pressure (single-component system) data in the literature. Importantly, the discrepancy between the two correlations is well outside the uncertainty range reported for the two equations, which $U(k = 2)$ are 1% and 2%, for the Huber et al. and Dumarey equations, respectively. Harvey et al.[36] used thermodynamic and molecular theory to calculate nonideal-gas and nonideal mixing behavior as well as the effect of pressure on the chemical potential of condensed phase. They predicted that the temperature-dependent saturated vapor concentration for the Hg−air two-component system should exhibit only a small correction from the single-component case, albeit in the reverse direction. This predicted correction factor for equilibrium mercury concentration caused by the presence of air ranged from 1.0025 at 0 °C to 1.0016 at 40 °C. Additional data available for comparison of Hg mass concentration at saturation is the recent work by Quétel et al.[37] involving development of an SI-traceable mass spectrometer method similar to that described in the introduction. They reported an expanded (combined) relative uncertainty, $U(k = 2)$, of 5.9% at 20 °C. Quétel et al. reported mercury concentration values nearly 3% and 10% higher by comparison to predictions (evaluated at 20 °C) based on the Huber et al. and Dumarey correlations, respectively. It suffices to say that the accuracy of the predicted GEM produced by a Hg-in-air generator depends strongly on the vapor pressure−temperature correlation utilized.

The absolute mass concentrations of Hg vapor derived from our measurements are compared (Table 1) to the concentrations, predicted using the vapor pressure function proposed by Huber et al. for pure Hg as well as the Dumarey equation for Hg saturated air. Additionally, we have included a comparison with the recent SI-traceable ID-ICPMS measurements by Quétel et al.[37] for Hg saturated air. In order to calculate the Hg mass concentrations at our temperature values (295.098−295.197) K, we have used a third-order polynomial interpolation to fit the ICPMS mass concentration versus temperature data (288.4−303.1) K. For the purposes of standard uncertainty calculation, we have used the combined relative standard uncertainty value (3%) reported in Quétel et al.[37]

Table 1. Comparison of Values of Our Measured Hg Vapor Mass Concentration with Various Vapor-Pressure Correlation Equations and Available SI-Traceable ID-ICPMS Data[a]

term	Hg-only	Hg−air	Hg−N_2
temperature, K	295.197 (0.100)	295.098 (0.047)	295.189 (0.094)
this work, mg m^{-3}	17.01 (0.22)	16.79 (0.25)	16.81 (0.14)
Huber et al., mg m^{-3}	16.67 (0.08)		
Dumarey, mg m^{-3}		15.59 (0.16)	
Quétel et al. mg m^{-3}		17.07 (0.50)	

[a]The standard uncertainty values are reported in brackets for temperature and mass concentration values, respectively.

Our measured vapor mass concentration for elemental mercury for Hg and Hg−air systems lie between those predicted by the Huber equation and Quétel et al.'s[37] SI-traceable ID-ICPMS results, respectively. They may be considered equivalent to both results within our experimental uncertainty. These results are consistent with the theoretical calculations of Harvey et al. where the Hg−air system near room temperature was predicted to have a saturated partial pressure approximately 0.2% greater than the Hg vapor pressure. In contrast, our value for Hg vapor pressure for Hg−air system is 8.5% higher than the value predicted from the Dumarey equation.

CONCLUDING REMARKS

We have demonstrated quantitative, high-resolution laser absorption spectroscopy of gaseous elemental mercury on the suite of ten 6 $^1S_0 \leftarrow 6\ ^3P_1$ transitions near $\lambda = 253.7$ nm that correspond to the seven stable isotopes of mercury. Samples considered included Doppler-broadened pure Hg vapor (Hg-only) as well as foreign broadened Hg−air and Hg−N_2 mixtures. For all three samples considered, we closely fit the observed composite spectra to a linear superposition of Voigt profiles at known absolute frequencies, calculated line intensities, and line shape parameters. Within an experimental relative standard uncertainty of 0.8−1.5%, we found that for all three samples, the measured amounts of mercury vapor are consistent with the most accurate thermodynamically constrained literature values for the vapor pressure of pure mercury. The measurement precision demonstrated here also indicates the potential for spectroscopic measurements of Hg isotopes at the few parts-per-thousand level.

The ability to model the observations from first-principles and the low combined uncertainty of our measurements establish the suitability of the present spectroscopic technique for absolute, SI-traceable measurements of Hg concentration. To build on the present work, we will investigate the temperature dependence for a static cell system and concurrently develop a system to measure Hg in saturated air or N_2 using a long-path, flow cell system. The goals will be to refine further the present comparison and to establish an accurate, sensitive, and rapid spectroscopic technique applicable to mercury-in-air standard concentration measurements.

Finally, we note that though our work is based on Hg^0 detection, use of known[38] and practiced sample reduction and desorption schemes can conceivably be added to determine the

DOI: 10.1021/acs.analchem.8b00757
Anal. Chem. XXXX, XXX, XXX−XXX

concentration of atmospherically relevant Hg(II) and Hg-p forms, respectively.

■ ASSOCIATED CONTENT

Supporting Information

The Supporting Information is available free of charge on the ACS Publications website at DOI: 10.1021/acs.analchem.8b00757.

S1, simulation of mercury absorption spectrum; Table S1.I, summary of mercury 6 $^1S_0$ ← 6 $^3P_1$ transitions; Figure S1.1, simulated spectrum for pure mercury vapor at T = 296 K; S2, saturation and photoreaction effects; Figure S2.1, dependence of integrated absorption on laser intensity for Hg, Hg−N_2, and Hg−air samples; S3, effect of multiple reflections and cell orientation; S4, uncertainty analysis; Table S4.I, number density combined standard relative uncertainty budget (PDF)

■ AUTHOR INFORMATION

Corresponding Author

*E-mail: abneesh.srivastava@nist.gov.

ORCID

Abneesh Srivastava: 0000-0002-8527-112X

Notes

The authors declare no competing financial interest.

■ ACKNOWLEDGMENTS

The authors would like to thank Drs. S. Long and E. Benck for carefully reviewing the manuscript.

■ REFERENCES

(1) Gworek, B.; Dmuchowski, W.; Baczewska, A. H.; Bragoszewska, P.; Bemowska-Kalabun, O.; Wrzosek-Jakubowska, J. *Water, Air, Soil Pollut.* **2017**, *228*, 31.

(2) Slemr, F.; Schuster, G.; Seiler, W. *J. Atmos. Chem.* **1985**, *3*, 407−434.

(3) Agnan, Y.; Le Dantec, T.; Moore, C. W.; Edwards, G. C.; Obrist, D. *Environ. Sci. Technol.* **2016**, *50*, 507−524.

(4) Driscoll, C. T.; Mason, R. P.; Chan, H. M.; Jacob, D. J.; Pirrone, N. *Environ. Sci. Technol.* **2013**, *47*, 4967−4983.

(5) Higueras, P.; Oyarzun, R.; Kotnik, J.; Esbri, J. M.; Martinez-Coronado, A.; Horvat, M.; Lopez-Berdonces, M. A.; Llanos, W.; Vaselli, O.; Nisi, B.; Mashyanov, N.; Ryzov, V.; Spiric, Z.; Panichev, N.; McCrindle, R.; Feng, X. B.; Fu, X. W.; Lillo, J.; Loredo, J.; Garcia, M. E.; et al. *Environ. Geochem. Health* **2014**, *36*, 713−734.

(6) Clarkson, T. W.; Magos, L. *Crit. Rev. Toxicol.* **2006**, *36*, 609−662.

(7) Grandjean, P.; Satoh, H.; Murata, K.; Eto, K. *Environ. Health Perspect.* **2010**, *118*, 1137−1145.

(8) European Commission. http://ec.europa.eu/environment/chemicals/mercury/.

(9) United States Environmental Protection Agency. https://www.epa.gov/mats.

(10) Agency for Toxic Substances and Disease Registry. https://www.atsdr.cdc.gov/toxprofiles/index.asp.

(11) EPA. *Method 30A-Determination of Total Vapor Phase Mercury Emissions From Stationary Sources.*

(12) Long, S. E.; Kelly, W. R. *Anal. Chem.* **2002**, *74*, 1477−1483.

(13) Fain, X.; Moosmuller, H.; Obrist, D. *Atmos. Chem. Phys.* **2010**, *10*, 2879−2892.

(14) Jongma, R. T.; Boogaarts, M. G. H.; Holleman, I.; Meijer, G. *Rev. Sci. Instrum.* **1995**, *66*, 2821−2828.

(15) Pierce, A.; Obrist, D.; Moosmuller, H.; Fain, X.; Moore, C. *Atmos. Meas. Tech.* **2013**, *6*, 1477−1489.

(16) Tao, S. Q.; Mazzotti, F. J.; Winstead, C. B.; Miller, G. P. *Analyst* **2000**, *125*, 1021−1023.

(17) Callear, A. B.; Patrick, C. R.; Robb, J. C. *Trans. Faraday Soc.* **1959**, *55*, 280−287.

(18) Granite, E. J.; Pennline, H. W. *Ind. Eng. Chem. Res.* **2002**, *41*, 5470−5476.

(19) Granite, E. J.; Pennline, H. W.; Hoffman, J. S. *Ind. Eng. Chem. Res.* **1999**, *38*, 5034−5037.

(20) Almog, G.; Scholz, M.; Weber, W.; Leisching, P.; Kaenders, W.; Udem, T. *Rev. Sci. Instrum.* **2015**, *86*, 033110.

(21) Alnis, J.; Gustafsson, U.; Somesfalean, G.; Svanberg, S. *Appl. Phys. Lett.* **2000**, *76*, 1234−1236.

(22) Anderson, T. N.; Magnuson, J. K.; Lucht, R. P. *Appl. Phys. B: Lasers Opt.* **2007**, *87*, 341−353.

(23) Carruthers, A. E.; Lake, T. K.; Shah, A.; Allen, J. W.; Sibbett, W.; Dholakia, K. *Opt. Commun.* **2005**, *255*, 261−266.

(24) Lou, X. T.; Zhang, T.; Lin, H. Z.; Gao, S. Y.; Xu, L. J.; Wang, J. N.; Wan, L.; He, S. L. *Opt. Express* **2016**, *24*, 27509−27520.

(25) Herzberg, G. *Atomic Spectra and Atomic Structure*; Dover Publications, 1944.

(26) De Laeter, J. R.; Bohlke, J. K.; De Bievre, P.; Hidaka, H.; Peiser, H. S.; Rosman, K. J. R.; Taylor, P. D. P. *Pure Appl. Chem.* **2003**, *75*, 683−800.

(27) Halstead, J. A.; Reeves, R. R. *J. Quant. Spectrosc. Radiat. Transfer* **1982**, *28*, 289−296.

(28) Curtis, L. J.; Irving, R. E.; Henderson, M.; Matulioniene, R.; Fischer, C. F.; Pinnington, E. H. *Phys. Rev. A: At., Mol., Opt. Phys.* **2001**, *63*, 7.

(29) Jacobs, J. P.; Warrington, R. B. *Phys. Rev. A: At., Mol., Opt. Phys.* **2003**, *68*, 6.

(30) Wcislo, P.; Cygan, A.; Lisak, D.; Ciurylo, R. *Phys. Rev. A: At., Mol., Opt. Phys.* **2013**, *88*, 8.

(31) Meija, J.; Yang, L.; Sturgeon, R. E.; Mester, Z. *J. Anal. At. Spectrom.* **2010**, *25*, 384−389.

(32) Brand, W. A.; Coplen, T. B.; Vogl, J.; Rosner, M.; Prohaska, T. *Pure Appl. Chem.* **2014**, *86*, 425−467.

(33) *Guides to the Expression of Uncertainty in Measurement* (GUM Series), http://www.iso.org/sites/JCGM/GUM-introduction.htm.

(34) Dumarey, R.; Brown, R. J. C.; Corns, W. T.; Brown, A. S.; Stockwell, P. B. *Accredit. Qual. Assur.* **2010**, *15*, 409−414.

(35) Huber, M. L.; Laesecke, A.; Friend, D. G. *Ind. Eng. Chem. Res.* **2006**, *45*, 7351−7361.

(36) Harvey, A. H. *Int. J. Thermophys.* **2010**, *31*, 297−307.

(37) Quetel, C. R.; Zampella, M.; Brown, R. J. C. *TrAC, Trends Anal. Chem.* **2016**, *85*, 81−88.

(38) Gustin, M. S.; Amos, H. M.; Huang, J.; Miller, M. B.; Heidecorn, K. *Atmos. Chem. Phys.* **2015**, *15*, 5697−5713.

DOI: 10.1021/acs.analchem.8b00757
Anal. Chem. XXXX, XXX, XXX−XXX